ACS APPLIED MATERIALS & INTERFACES

RESEARCH ARTICLE

www.acsami.org

Template-Free Synthesis of Hierarchical TiO_2 Structures and Their Application in Dye-Sensitized Solar Cells

Fang Shao, Jing Sun,* Lian Gao, Songwang Yang, and Jianqiang Luo

The State Key Lab of High Performance Ceramics and Superfine Microstructure, Shanghai Institute of Ceramics, Chinese Academy of Sciences, 1295 Ding Xi Road, Shanghai 200050, China

Supporting Information

ABSTRACT: We demonstrate here the synthesis of a hierarchical TiO_2 architecture without any surfactants or templates. Two kinds of structure existed simultaneously, the ordered nanoarrays at bottom provided direct conduction pathway for photo generated electrons, while the upper micro-flowers consisted of nanobelt as building units increased the light harvesting ability as the scattering part. The formation mechanism of the hierarchical architecture has been proposed by studying the morphology evolution processes upon reaction time. The performance of dye-sensitized solar cells based on the obtained hierarchical anatase TiO_2 has been also studied, giving a J_{SC} = 12.44 mA cm^{-2}, V_{OC} = 0.64 V, FF = 69.05%, and η = 5.53%, which is superior than commercial TiO_2 (P25). The UV−vis results prove that the obtained morphology is beneficial to light-scattering and thus increases the light harvesting ability. This hierarchical TiO_2 structure offers great potential for the development of high-efficiency DSSCs.

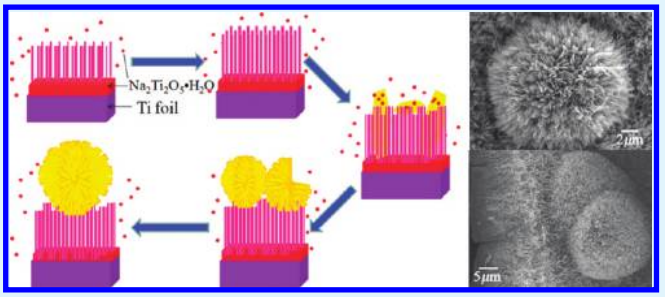

KEYWORDS: hierarchical, titania, photoanode, dye-sensitized solar cells, light harvesting

INTRODUCTION

Metal oxide nanostructures represent a particularly interesting class of materials for widespread applications. In recent years, the control over morphology and structure of metal oxide materials has attracted much attention because their physical and chemical properties depend considerably on the morphology, structure, phase, shape, size, and dimensionality.[1−4] Among them, titanium dioxide (TiO_2) is of intense interest due to its applications in photocatalysts, self-cleaning devices, gas sensors, and dye-sensitized solar cells (DSSCs), etc.[5−12] Up to now, TiO_2 with various morphologies has been synthesized, such as nanoparticles, nanorods, nanospheres, and so on.[13−17] Among these, self-assembly of 1D nanostructure into hierarchical 3D architecture has attracted extensive attention because they may exhibit interesting properties because of the large numbers of active sites, unique multidimensional morphology, and the combination of micro-nano scales.[18] In solar cells, 1D TiO_2 nanostructures can accelerate the movement of electrons in one direction and reduce their recombination.[19,20] Fu et al. prepared 3D hierarchical flower-like TiO_2 nanostructure with an average diameter of ∼1.5 μm, they also demonstrated that this structure had better photocatalytic activity compared with P25.[21] But this structure may not be appropriate for anode in DSSCs owing to their poor dye-loading capacity.[22] However, when being used as a scattering layer, it can increase the cells' performance by enhancing the light harvesting.

The ability of light harvesting is also important for working electrodes while many TiO_2 nanostructures are very weak scatterers. Therefore, the double-layered structures with a scattering layer have been widely employed to improve the light harvesting ability and thus enhance the efficiency of the solar cell.[23,24] However the films were obtained by doctor-blade casting several times, which increased the complexity of the process.

Therefore, it is meaningful to fabricate hierarchical TiO_2 photoanodes with both high light harvesting and good transferring properties. To date, researches have focused on developing methods to produce hierarchically structured TiO_2 whereas surfactants or templates were needed in many procedures.[2,25−28] For the purpose to be used as anodes, additives applied will decrease the efficiency and make the process complex. Moreover, to the best of our knowledge, study of the TiO_2 photoanodes consisting of both 1D nanoarray and 3D hierarchical structures has not yet been reported. Even though Chen et al.[28] have mentioned the morphology that some flower-like structures were formed on top of the nanowire films, many fundamental aspects, such as the formation mechanism of the structure, the detachment of the thin film, the preparation of photoanodes and the performance of device based on the hierarchical TiO_2, have not been adequately assessed.

In this study, we report the successful fabrication of hierarchical TiO_2 for DSSCs. As a synthetic tool, we used an alkaline hydrothermal treatment in which many experiment parameters can be easily and flexibly tuned. The obtained TiO_2 has two kinds

Received: March 26, 2011
Accepted: May 10, 2011
Published: May 10, 2011

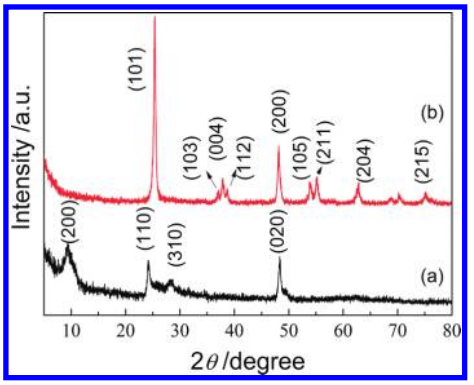

Figure 1. XRD patterns of the samples (a) before calcination step and (b) after being calcinated at 500°C for 30 min.

of morphologies, one is nanowire array and another is microflowers consisting of nanobelt building blocks. The obtained structures were detached from Ti foils and adhered onto FTO glasses to form photoanodes in DSSCs, and the power conversion efficiency (η) of 5.53% was obtained with a short-circuit current (J_{SC}) of 12.44 mA cm^{-2}, an open-circuit voltage (V_{OC}) of 0.64 V, and a fill factor (FF) of 69.05%.

EXPERIMENTAL SECTION

Synthesis and Characterization of Hierarchical Architectures. Titanium foils (99.97% purity, 0.25 mm thickness, Sigma-Aldrich) were first ultrasonically cleaned with deionized water, ethanol, and acetone for 30 min, respectively. After drying, they were placed at an angle against the wall of Teflon-lined stainless steel autoclave. Inside, there was 25 mL of 5 M NaOH aqueous solution. The hydrothermal synthesis was carried out at 220 °C for 24 h in an electric oven. After reaction, the samples were washed with deionized water and ethanol for several times and dried in oven. They were then treated according to a previously reported procedure.[28−30] After immersing in 0.6 M HCl for 2 h, the Na^+ of samples was exchanged with H^+. The samples could be easily peeled off from the Ti substrate as membranes by placing in 0.6 M HCl overnight. They were calcinated at 500 °C for 30 min to convert to TiO_2. The time-dependent experiments were carried out at 220 °C with reaction time varied from 4 h to 48 h.

The crystal structures were examined by X-ray diffraction (XRD, D/max 2550 V, Rigaku Tokyo, Japan). Morphological and lattice structural information were examined with field emission scanning electron microscopy (FESEM, JSM-6700F, JEOL Tokyo, Japan), transmission electron microscopy (TEM/HRTEM, JEM-200CX, JEOL Tokyo, Japan) and selected area electron diffraction (SAED). The composition and contents of the obtained samples were investigated by energy dispersive spectrometer (EDS). The specific surface area of products was estimated by the Brunauer−Emmet−Teller (BET) method based on nitrogen adsorption (Micromeritics ASAP 2020).

Fabrication and Characterization of DSSCs. The photovoltaic performance of the obtained TiO_2 films was investigated by measuring the DSSCs using the films as working electrodes. The substrates (FTO coated glasses) were firstly prepared by depositing a thin layer of nanocrystalline TiO_2 paste (~260 nm) onto FTO using screen printing method. The as prepared sample was then peeled off from the Ti plates as membranes, and pasted onto the FTO glasses. After being dried under ambient conditions, the samples were annealed at 500°C for 30 min. Prior to dye adsorption, the $TiCl_4$ post-treatment was carried out. The obtained samples were dipped into 0.2 M $TiCl_4$ solution at 60°C for 1 h and washed with water and ethanol. After drying, the FTOs coated with TiO_2 films were gradually calcinated at 450°C for 30 min.

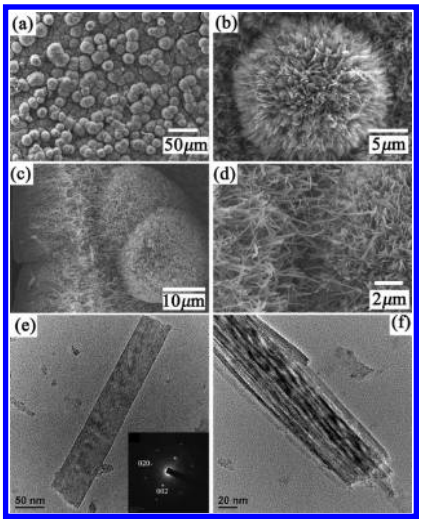

Figure 2. SEM and TEM images of $H_2Ti_2O_5 \cdot H_2O$ grown for 24 h: (a) top views; (b) a selected sphere; (c) cross-sectional views; (d) the enlarged junction of nanoarrays and a microsphere; (e) TEM image of a single nanobelt and the corresponding SAED pattern; (f) TEM image of the nanowire.

The dye used in this work was *cis*-bis(isothiocyanato) bis(2, 2′-bipyridyl-4-4′-dicarboxylato)-ruthenium(II)bis-tetrabuty-lammonium, called N719 hereafter. N719 was absorbed onto the surface of the TiO_2 films by immersing the samples in dye solution (concentration, 0.3 mM; solvent mixture, acetonitrile and *tert*-butyl alcohol in a volume ratio of 1:1) for 24 h. The dye-covered TiO_2 electrode and Pt-covered FTO glass counter electrode were assembled into a sandwich type cell. Liquid electrolyte was injected into the space between the photoanode and the counter electrode. Then, the DSSC cell was obtained. The electrolyte had the following composition: 0.5 M LiI, 0.05 M I_2, and 0.5 M tert-butylpyridine in acetonitrile. Photovoltaic properties were measured with an electrochemical workstation (Model CHI660C, CH) under an AM1.5 illumination (100 mW/cm^2, Model YSS-80A, Yamashita). Prior to measurements, an aperture mask with area of 0.10 cm^2 was employed for the calibration of the cell area. Reflectance spectra of the TiO_2-covered FTOs were obtained by an UV−vis spectrometer (Lambda 950, Perkin-Elmer, Waltham, MA).

RESULTS AND DISCUSSION

Figure 1 displays the XRD patterns of the synthesized thin film before and after calcination. The XRD pattern from the film treated by hydrothermal reaction and ion exchange process could be indexed to orthorhombic hydrated dititanate ($H_2Ti_2O_5 \cdot H_2O$, JCPDS card No. 47-0124). The XRD pattern shown in Figure 1b matches well with the crystal structure of the anatase TiO_2 phase (JCPDS card No.21-1272) and no other phase is observed, all of these indicate that after being calcinated at 500°C for 30 min, $H_2Ti_2O_5 \cdot H_2O$ has been completely converted to anatase TiO_2. The sharp and intense peaks reveal that the obtained TiO_2 is well crystallized.

The morphology of $H_2Ti_2O_5 \cdot H_2O$ hydrothermally synthesized in 5 M NaOH aqueous for 24 h is shown in Figure 2. The images reveal that the obtained structure is composed of two parts. The upper part contains microflowers with diameter about 15−25 μm. The bottom is made up of oriented nanowire arrays, which are perpendicular to the titanium substrate. The microflowers are in fact hierarchical architectures composed of nanobelts. The microflowers exhibit open structures with numerous

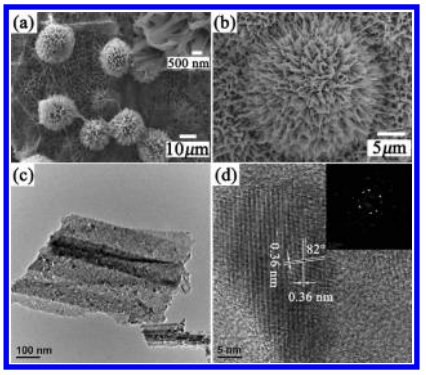

Figure 3. (a, b) Low and high-magnification top view SEM images of the obtained anatase TiO_2 after being calcinated at 500°C for 30 min; (c) TEM image of TiO_2 nanobelts which overlap each other; and (d) HRTEM image and the corresponding SAED pattern taken from (c).

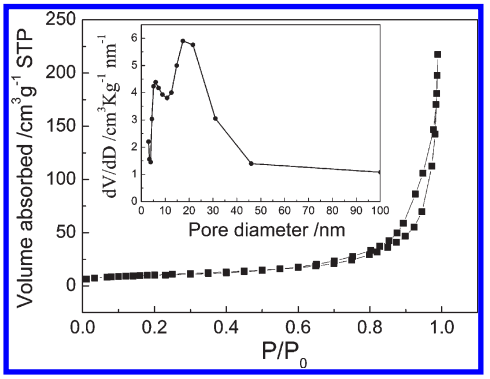

Figure 4. N_2 adsorption/desorption isotherm of the as-prepared anatase TiO_2. The inset image shows the pore size distributions calculated from the desorption branch of a nitrogen isotherm by the BJH method.

nanobelts extended outside, and become gradually compact inside. This open structures can enhance the absorption of light and thus improve the performance of DSSCs.[31] The nanobelts in flowers of upper part are much wider than nanowires arrays on the bottom; and good connection between the two structures could be observed in Figure 2d. From Figure 2e, we can see that the nanobelts are of single crystalline and grow along the [001] direction. Figure 2f indicates that the nanowires have multi-layered structure. The diameter of the nanowires, as determined from SEM and TEM images, is in the order of 50−100 nm and the typical length is about 12 μm. From Figure 3, we can clearly see that after heat treatment, the as prepared morphology is not damaged. The building units of microspheres are still nanobelts and the open-ended structure is preserved. The tips of nanobelts and nanaowires bend and stick together to form a structure with macropores which cannot be detected by nitrogen adsorption/desorption measurements. The bending of the tips is because of the tendency of releasing surface free energy during the calcination.[30] Part of nanobelts is shown in Figure 3c, from which we can see that the thin nanobelts have rough surface. The corresponding HRTEM image (Figure 3d) exhibits visible lattice fringes. There are two sets of lattices and the angle between them is about 82°. The interfringe spacings are both 0.36 nm, which corresponding to anatase (101) and (011) planes. The SAED pattern in Figure 3d indicates good crystallinity of the nanobelt which accords well with the result of XRD. There are also

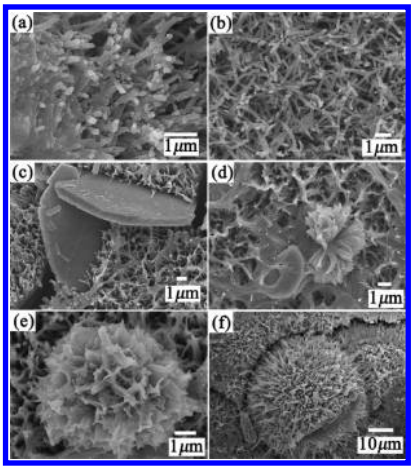

Figure 5. Top view SEM images of the $H_2Ti_2O_5 \cdot H_2O$ structures grown for (a) 4 h; (b) 10 h; (c)16 h; (d,e) 20 h; (f) 48 h.

multilayer nanowires, as shown in Supporting Information, Figure S1. Additionally, the composition and contents of the sample were investigated by EDS measurements. The EDS results (Supporting Information, Figure S2) reveal that Ti and O are the only elementary components and their concentrations are 34.74 and 65.26 atom %, respectively. We can see the atomic ratio of Ti and O is about 1:2.

The mesoporous nature of the hierarchical TiO_2 can be quantified with nitrogen adsorption/desorption measurements and the corresponding pore size distribution is shown in Figure 4. The two hysteresis loops indicate that there are both small and large mesopores, which can be confirmed by the pore size distribution curve in the inset image. The pore size distribution ranged between 5 and 40 nm, and the average pore diameter is 25.9 nm. The BET surface area is 36.93 m^2/g while the volume of pores has a high number of 0.34 cm^3/g. Such porosity may be created by the dehydration process during phase transformation.

In order to investigate the formation mechanism of the hierarchical TiO_2 architectures, detailed time-dependent experiments were carried out at 220°C. From the SEM images of these products shown in Figure 5, the morphology evolution of the TiO_2 nanostructure is observed clearly. The growth time of 4 h resulted in the formation of oriented $H_2Ti_2O_5 \cdot H_2O$ nanowires as shown in Figure 5a, the length of nanowires (the thickness of the nanowires film) was about 4.5 μm. The shape did not change significantly at 10 h while the diameter and length were both increased (Figure 5b). From Figure 5c, we can see that sheets with thickness of about 0.5 μm appeared at 16 h, and they grew from the bottom. The low-magnification image revealed that size and shape of the sheets were not uniform (Supporting Information, Figure S3). There were various morphologies of the sample obtained at 20 h: thick sheets, nanowires, incomplete flowers composed of nanobelts and microflowers with the average diameter of 5 μm (Figure 5d, e). It's worth noting that no thick sheets could be observed both in SEM or TEM images when the reaction time came to 24 h, as shown in Figure 2. The flowers grew larger with the prolongation of treating time; the typical diameter of micro flowers was 46 μm at 48 h (Figure 5f).

Details of the sample grown for 16 h were investigated for further understanding the formation process. Figure 6 shows the TEM images of the multi-layered nanowires and a single sheet with the corresponding SAED patterns. Figure 6a reveals that

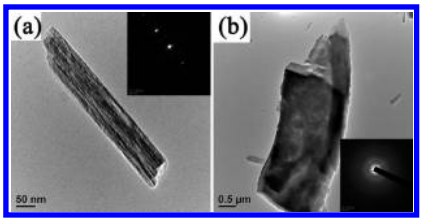

Figure 6. TEM images of the sample grown for 16 h (a) a part of nanowire and (b) a single sheet. Inset: the corresponding SAED patterns.

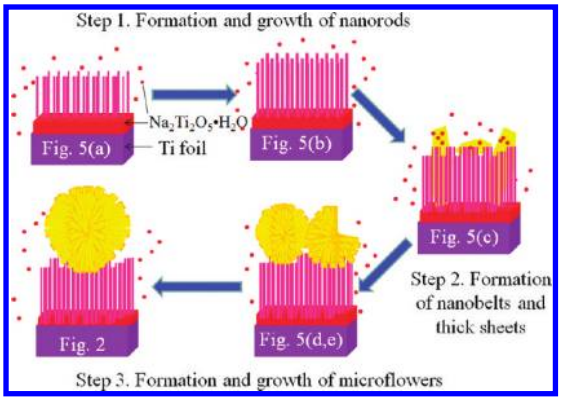

Figure 7. Schematic procedure for the formation of the hierarchical architectures.

crystallized multi-layed nanowires have been formed at this time. This structure may be resulted from the dislocations and defects in the nanowires. When nanowires are long enough, the defect strain is large enough to transform nanowires into multilayered structures.[29] On the other hand, as shown in Figure 6b, the sheet is not well crystallized, which is significantly different from nanowires. EDS results indicate that the Ti and O concentrations are 64 and 36 atom % in thick sheets (Supporting Information, Figure S4) while 27.25 and 72.75 atom % in nanowires (Supporting Information, Figure S5). Therefore, it can be deduced that the appearance of thick sheets may be due to the decrease of O on the surface of titanium substrate. As time goes on, it becomes more and more difficult for NaOH to diffuse to the titanium foil surface. Thus, thick sheets grew up from the bottom.

On the basis of the above experimental facts, we propose the following mechanism which is illustrated in Figure 7. The formation process based on the experimental results can be divided into three steps: (i) formation and growth of nanowires; (ii) formation of nanobelt and thick sheets; and (iii) formation and growth of microflowers. A dissolution-recrystallization-growth process may dominate the whole process. In the first step, the titanium foil acted both as the Ti source and the substrate. Ti atoms on the surface reacted with NaOH to form $Na_2Ti_2O_5 \cdot H_2O$ nanocrystallines which covered the substrate. Then, the nanocrystallized $Na_2Ti_2O_5 \cdot H_2O$ transformed into nuclei, and nanowires began to grow from them as a result of the hydrothermal treatment. Meanwhile, the Ti atoms inside diffused to the surface to supply Ti source. The nanowires were well oriented and nearly perpendicular to the substrate, since there were too many nuclei to grow in the cross direction. At last, oriented nanowires were obtained with the aid of selective

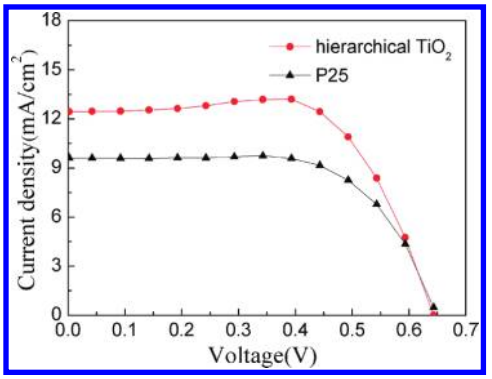

Figure 8. Photocurrent density−voltage curves for DSSCs fabricated from the hierarchical TiO_2 and P25 under AM1.5G simulated sunlight with a power density of 100 mW cm^{-2}.

absorptions of OH^-. This process can be explained by "nucleation-dissolution-recrystallization" growth mechanism. In the same period, the $Na_2Ti_2O_5 \cdot H_2O$ diffused to the solution, providing conditions for the subsequent step. After the hydrothermal treatment, there were white precipitates not only on titanium foils but also in the solution and on the wall of Teflon-lined autoclave, indicating that the $Na_2Ti_2O_5 \cdot H_2O$ could diffuse into the solution. Defect strain increased with the growth of nanowires, and when the strain was too large to bear, multi-layered nanowires were obtained. Meanwhile, thick sheets were formed probably by the reaction between Ti and the $Na_2Ti_2O_5 \cdot H_2O$. Subsequently, $Na_2Ti_2O_5 \cdot H_2O$ dissolved in the solution recrystallized on the surfaces of the former metastable sheets and nanobelts began to grow in all directions. At the same time, the sheets were gradually dissolved because of the alkaline condition and provided Ti ions to form nanobelts. Because there was no substrate to anchor the nanobelts, flower-like microspheres were formed step by step. The microflowers grew larger with time prolongation. On the contrary, the thick sheets were diminished gradually until completely disappeared.

The DSSCs were assembled from the hierarchical TiO_2 structures corresponding to Figure 3. At the same time, the compared experiments were also performed using the DSSCs based on P25 (Degussa). For more impartial comparison, we used the same TiO_2 nanocrystalline layer with similar thickness. And the overall thicknesses of the two samples were nearly same, as measured by a surface profile system (ORIX Rentec (Tianjin) Corporation). Figure 8 compares the solar cell response based on the two TiO_2 samples and the resultant photovoltaic parameters are summarized in Table 1. The DSSC with hierarchical TiO_2 photoanode presents superior performance. Compared with P25-DSSC, the amount of dye absorption was higher, the short-circuit current (J_{SC}) was enhanced from 9.61 to 12.44 mA cm^{-2}, and the efficiency was also increased from 4.10% to 5.53%.

Generally, the J_{SC} in DSSCs is dependent on the light harvesting efficiency, charge injection yield, and charge transport properties.[3] The charge injection yield lies on the relative energy levels of the dye and TiO_2, which is constant for a given material system. The traditional electrodes composed of TiO_2 particles are believed to limit the electron diffusion coefficient due to the trapping events at the contacts between nanoparticles. Instead, the 1D nanowires and nanobelts can significantly enhance the electron transport properties by providing the direct conduction pathways and greatly reducing inter-crystalline contacts.[32]

Table 1. Characteristics of DSSCs Based on Photoanodes of Hierarchical TiO_2 and P25

photoanodes	V_{OC} (V)	J_{SC} (mA cm^{-2})	FF (%)	η (%)	thickness (μm)	amount of dye[a] (μmol cm^{-2})
Hierarchical TiO_2	0.64	12.44	69.05	5.53	24.58	0.022
P25	0.65	9.61	65.89	4.10	24.87	0.017

[a] The dye-immersed photoanodes were soaked in a 0.1 M NaOH aqueous solution to desorb the dye. The amount of desorbed dye was quantified by measuring the optical absorption spectra.

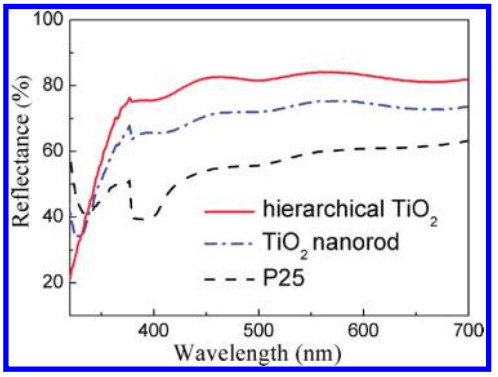

Figure 9. Reflectance spectra of the three different TiO_2 samples on FTOs.

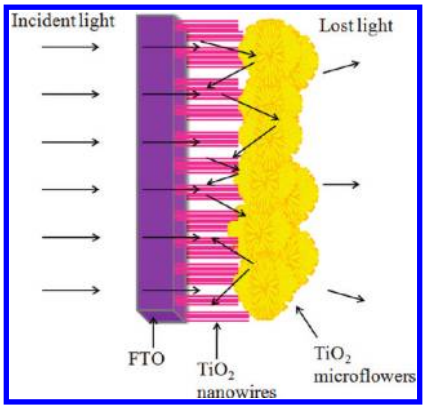

Figure 10. Schematic diagram of the light capture of TiO_2 microflowers as the scattering part in a cell.

The ability of light harvesting is very important for DSSCs while TiO_2 films made of nanoparticles usually exhibit high transparency and weak light scattering capability. The enhanced light scattering could confine the incident light in electrodes and thus plays a significant role in improving the light-harvesting efficiency.[23] Compared with the reflectance of the P25 TiO_2 film and the TiO_2 nanowires obtained by calcining the $H_2Ti_2O_5 \cdot H_2O$ grown for 10 h, the hierarchical TiO_2 film had the best diffuse reflection capability in the visible and near-infrared regions (Figure 9). It reflects that the unique hierarchical TiO_2 structure is in favor of enhancing the light scattering ability. The effect of the hierarchical structures on light absorption is illustrated in Figure 10. Though TiO_2 nanowire arrays without microfloweres exhibited better reflection than P25, the light loss in them is significant because many photons could pass through the gaps between adjacent nanowires. Instead, the incident light could be reflected for many times by microflowers, which would enhance the light harvesting ability.

The preparation of hierarchically structures is desirable for the application in DSSCs. Recently, the fabrication of hierarchical nanoporous TiO_2 or ZnO spheres for DSSCs has made some progress.[13,22,33,34] In spite of the high efficiency of such cells, the TiO_2 photoanodes contained 1D structures are expected to further improve the DSSCs' performance.[9,19,20] Hierarchical TiO_2 nanoarrays have also been developed as photoanodes. The optimized conversion efficiency of the reported DSSCs based on such structures is 4.9% and 5.7%, with thickness of 7 μm and 20 μm respectively.[35,36] However, the light harvesting ability was not well considered and the process is either too expensive or too time consuming. Here, after a simple three-step treatment, we successfully obtained the hierarchically structures combining both 1D nanowires and 3D microflowers, and they are beneficial to electron transport and light harvesting. Using these structures in DSSCs, we achieved 5.53% conversion efficiency.

CONCLUSION

In summary, the morphology of nanoarrays-microflowers hierarchical TiO_2 was synthesized without any surfactants or templates. The dissolution−recrystallization−growth formation mechanism of the hierarchical architectures was also proposed. When used in dye-sensitized solar cells, the build blocks of the obtained TiO_2 provide direct electrical pathways for photogenerated electrons, while the entire structure boosts the dye absorption and enhances the light harvesting ability, they together push further the power conversion efficiency. Finally, the DSSC using hierarchical TiO_2 electrode exhibits enhanced solar cell performance compared with P25 electrode.

ASSOCIATED CONTENT

Supporting Information. TEM images of TiO_2 nanowires, EDS scan of the obtained samples, and SEM image of the sample grown for 16 h. This material is available free of charge via the Internet at http://pubs.acs.org.

AUTHOR INFORMATION

Corresponding Author

*Tel.: +86-21-52414301. Fax: +86-21-52414903. E-mail: jingsun@mail.sic.ac.cn.

ACKNOWLEDGMENT

This work was supported by the National Natural Science Foundation of China (Grant No. 50972157, 51072215).

REFERENCES

(1) Kumar, A.; Madaria, A. R.; Zhou, C. W. *J. Phys. Chem. C* **2010**, *114*, 7787–7792.

(2) Chen, J. S.; Tan, Y. L.; Li, C. M.; Cheah, Y. L.; Luan, D. Y.; Madhavi, S.; Boey, F. Y. C.; Archer, L. A.; Lou, X. W. *J. Am. Chem. Soc.* **2010**, *132*, 6124–6130.

(3) Xu, F.; Dai, M.; Lu, Y. N.; Sun, L. T. *J. Phys. Chem. C* **2010**, *114*, 2776–2782.

(4) Park, K.; Zhang, Q. F.; Garcia, B. B.; Zhou, X. Y.; Jeong, Y. H.; Cao, G. Z. *Adv. Mater.* **2010**, *22*, 2329–2332.

(5) Yin, S.; Aita, Y.; Komatsu, M.; Wang, J. S.; Tang, Q.; Sato, T. *J. Mater. Chem.* **2005**, *15*, 674–682.
(6) Wu, Z.; Lee, D.; Rubner, M. F.; Cohen, R. E. *Small* **2007**, *3*, 1445–1451.
(7) Gong, J.; Li, Y. H.; Hu, Z. S.; Zhou, Z. Z.; Deng, Y. L. *J. Phys. Chem. C* **2010**, *114*, 9970–9974.
(8) Kim, D.; Lee, K.; Roy, P.; Birajdar, B. I.; Spiecker, E.; Schmuki, P. *Angew. Chem., Int. Ed.* **2009**, *48*, 9326–9329.
(9) Kang, T. S.; Smith, A. P.; Taylor, B. E.; Durstock, M. F. *Nano Lett.* **2009**, *9*, 601–606.
(10) Chen, J. K.; Li, K. X.; Luo, Y. H.; Guo, X. Z.; Li, D. M.; Deng, M. H.; Huang, S. Q.; Meng, Q. B. *Carbon* **2009**, *47*, 2704–2708.
(11) Song, Y. Y.; Schmidt-Stein, F.; Berger, S.; Schmuki, P. *Small* **2010**, *6*, 1180–1184.
(12) Kuang, D.; Brillet, J.; Chen, P.; Takata, M.; Uchida, S.; Miura, H.; Sumioka, K.; Zakeeruddin, S. M.; Gratzel, M. *ACS Nano* **2008**, *2*, 1113–1116.
(13) Sauvage, F.; Chen, D. H.; Comte, P.; Huang, F. Z.; Heiniger, L. P.; Cheng, Y. B.; Caruso, R. A.; Graetzel, M. *ACS Nano* **2010**, *4*, 4420–4425.
(14) Oh, J. K.; Lee, J. K.; Kim, H. S.; Han, S. B.; Park, K. W. *Chem. Mater.* **2010**, *22*, 1114–1118.
(15) Yang, H. G.; Liu, G.; Qiao, S. Z.; Sun, C. H.; Jin, Y. G.; Smith, S. C.; Zou, J.; Cheng, H. M.; Lu, G. Q. *J. Am. Chem. Soc.* **2009**, *131*, 4078–4083.
(16) Chen, D. H.; Huang, F. Z.; Cheng, Y. B.; Caruso, R. A. *Adv. Mater.* **2009**, *21*, 2206–2210.
(17) Liu, Y.; Wang, H.; Li, M.; Hong, R. J.; Ye, Q. H.; Zheng, J. M.; Shen, H. *Appl. Phys. Lett.* **2009**, *95*, 233505.
(18) Hu, X. L.; Yu, J. C.; Gong, J. M. *J. Phys. Chem. C* **2007**, *111*, 11180–11185.
(19) Liu, B.; Aydil, E. S. *J. Am. Chem. Soc.* **2009**, *131*, 3985–3990.
(20) Feng, X. J.; Shankar, K.; Varghese, O. K.; Paulose, M.; Latempa, T. J.; Grimes, C. A. *Nano Lett.* **2008**, *8*, 3781–3786.
(21) Tian, G. H.; Chen, Y. J.; Zhou, W.; Pan, K.; Tian, C. G.; Huang, X. R.; Fu, H. G. *CrystEngComm* **2011**, *13*, 2994–3000.
(22) Zhang, Q. F.; Chou, T. R.; Russo, B.; Jenekhe, S. A.; Cao, G. Z. *Angew. Chem., Int. Ed.* **2008**, *47*, 2402–2406.
(23) Qiu, Y. C.; Chen, W.; Yang, S. H. *Angew. Chem., Int. Ed.* **2010**, *49*, 3675–3679.
(24) Huang, F. Z.; Chen, D. H.; Zhang, X. L.; Caruso, R. A.; Cheng, Y. B. *Adv. Funct. Mater.* **2010**, *20*, 1301–1305.
(25) Hou, J. G.; Qu, Y. F.; Krsmanovic, D.; Ducati, C.; Eder, D.; Kumar, R. V. *J. Mater. Chem.* **2010**, *20*, 2418–2423.
(26) Yang, W. G.; Wan, F. R.; Wang, Y. L.; Jiang, C. H. *Appl. Phys. Lett.* **2009**, *95*, 133121.
(27) Huang, J. Q.; Huang, Z.; Guo, W.; Wang, M. L.; Cao, Y. G.; Hong, M. C. *Cryst. Growth Des.* **2008**, *8*, 2444–2446.
(28) Peng, X. S.; Chen, A. C. *Adv. Funct. Mater.* **2006**, *16*, 1355–1362.
(29) Wang, W. L.; Lin, H.; Li, J. B.; Wang, N. *J. Am. Ceram. Soc.* **2008**, *91*,
628–631.
(30) Liu, B.; Boercker, J. E.; Aydil, E. S. *Nanotechnology* **2008**, *19*, 505604.
(31) Yu, J. G.; Su, Y. R.; Cheng, B. *Adv. Funct. Mater.* **2007**, *17*, 1984–1990.
(32) Kang, S. H.; Choi, S. H.; Kang, M. S.; Kim, J. Y.; Kim, H. S.; Hyeon, T.; Sung, Y. E. *Adv. Mater.* **2008**, *20*, 54–58.
(33) Kim, Y. J.; Lee, M. H.; Kim, H. J.; Lim, G.; Choi, Y. S.; Park, N. G.; Kim, K.; Lee, W. I. *Adv. Mater.* **2009**, *21*, 3668–3673.
(34) Zhang, Q. F.; Cao, G. Z. *J. Mater. Chem.* **2011**, *21*, 6769–6774.
(35) Sauvage, F.; Di Fonzo, F.; Bassi, A. L.; Casari, C. S.; Russo, V.; Divitini, G.; Ducati, C.; Bottani, C. E.; Comte, P.; Graetzel, M. *Nano Lett.* **2010**, *10*, 2562–2567.
(36) Zhuge, F. W.; Qiu, J. J.; Li, X. M.; Gao, X. D.; Gan, X. Y.; Yu, W. D. *Adv. Mater.* **2011**, *23*, 1330–1334.